Multiple rainbow singularities in product rotational distributions of exothermic collisions: A probe for the P_4 anisotropy of the system $Ar(^1S_0)+N_2(C\,^3\Pi_u)$

E. J. D. Vredenbregt, M. R. van den Bogaard,* and H. C. W. Beijerinck
Department of Physics, Eindhoven University of Technology, P.O. Box 513, 5600 MB Eindhoven, The Netherlands
(Received 19 January 1988; revised manuscript received 10 February 1989)

The effect on product rotational distributions of the energy released during exothermic processes is investigated with the model of collisions with a rigid, anisotropic shell. With increasing exothermicity, rotational-rainbow maxima become apparent in model integral cross sections for rotational excitation, due to the increasing importance of the final-state repulsion with respect to that in the initial state. Such rainbow maxima are expected to occur in product distributions of excitation transfer, chemical reactions, and dissociation processes. Two different rotational-rainbow maxima can appear even for homonuclear product molecules when the interaction potential contains substantial anisotropy described by a fourth-order Legendre polynomial P_4. This type of anisotropy can explain the bimodal rotational distribution of the product $N_2(C)$ of the exothermic excitation-transfer collision $Ar^*(^3P_{0,2})+N_2(X)$, with an energy release $\Delta E=701$ and 521 meV for the $^3P_0$ and $^3P_2$ states, respectively, as measured by Nguyen and Sadeghi at a temperature of 90 K (=11 meV). The scaling of the rainbow positions with the exothermicity is reproduced. The best agreement with the experimental data is obtained with a ratio of anisotropy parameters $c_4/c_2=1.8$. Such anisotropy may be caused by the promotion of a $2\sigma_u$ electron to a $2\pi_g$ orbital when going from the X to the C state of N_2.

I. INTRODUCTION

The dramatic effect of rotational-rainbow singularities on product rotational distributions was first clearly demonstrated by Beck, Schepper, and Ross in energy-loss spectra of K atoms colliding with CO and N_2.[1] Since then, experimental data on rotational state-to-rotational state differential cross sections collected by several groups, noticeably that of Bergmann,[2–4] have shown the importance of the concept of rotational rainbows for understanding rotational energy transfer in ion-,[5] atom-,[6] molecule-,[7] and even electron-[4] molecule collisions.

Generally,[8] final rotational state j' selected differential cross sections $\partial\sigma(\vartheta,j')/\partial\vartheta$ display a maximum at the rainbow angle $\vartheta_R(j')$ followed by secondary maxima at larger values of ϑ if sufficient resolution is available.[3,8] Conversely, at fixed scattering angle, the product rotational state of the molecule or, equivalently, the energy loss of the primary colliding species, shows maximum probability near the maximum transferred angular-momentum quantum $\Delta\mathbf{j}=\mathbf{j}'-\mathbf{j}$,[8] with $\mathbf{j}'$ the final and $\mathbf{j}$ the initial rotational angular momentum.

As shown by Beck and co-workers,[1,9] the appearance of these maxima can be understood on the basis of classical scattering of a structureless particle from a rigid, anisotropic potential shell. The maxima are the result of roots of the Jacobian $|\partial(\vartheta,j')/\partial(b,\gamma)|$ for fixed scattering angle ϑ or fixed rotational state j' as a function of the impact parameter b and orientation angle γ.

The predictions of this model are confirmed by semiclassical and quantal calculations. A model study by Korsch and Schinke,[10] mimicking the scattering of He by Na_2 at a collision energy $E=100$ meV, shows that not only the classical treatment of the collision, but also the replacement of the full potential by a rigid shell, still leaves the model of Beck and co-workers in qualitative agreement with semiclassical and quantal calculations for the system. In other theoretical studies as well, rotational-rainbow maxima are apparent in differential cross sections.[3,8,11,12] The interpretation of such maxima in terms of rotational-rainbow maxima is therefore now well established.

While rotational rainbows are common in differential cross sections, for systems without energy release they do not show up as pronounced features in product rotational distributions, i.e., in the integral cross section $\sigma(j')$.[10,13] This is due to the strong dependence of the rainbow state j'_R on the scattering angle ϑ, as is predicted by the approximate relation[8,12]

$$j'_R(\vartheta)=j'_R(\pi)\sin(\vartheta/2)\ . \tag{1}$$

Integration of the differential cross section with respect to ϑ to obtain the integral cross section, thus largely averages out the marked rainbow features. All that remains is a shoulder for large j'. Therefore, a rainbow analysis of integral rotational distributions for collisions without energy release does not seem useful.

In this paper we show that this averaging works out very differently for collisions having a large energy release on the exit-channel potential and a fairly flat entrance-channel potential. A limiting case is formed by half collisions, e.g., the photodissociation of molecules, where the entrance channel is entirely missing. For such cases, we expect always to find marked rainbow maxima

 ©1989 The American Physical Society

in integral product rotational distributions at large angular-momentum transfer. For photodissociation, this has already been identified by Schinke for $H_2CO \rightarrow H_2 + CO$,[14] by Sato *et al.* for the van der Waals molecules Ar $\cdots$ NO and Ne $\cdots$ NO (Ref. 15) and possibly by Cline *et al.* for He $\cdots$ Cl_2.[16] This rainbow effect is probably responsible for high j' maxima in rotational distributions of various chemical reactions as well. Rainbow maxima show up in integral cross sections for such cases because the rotational excitation is mainly determined by the repulsion on the exit-channel potential. The entrance channel plays a minor role because of the energy release in the second half of the collision. In the extreme case that $\Delta E/E \gg 1$, with ΔE the exothermicity and E the collision energy, the rainbow position $j'_R(\vartheta)$ will no longer depend on the scattering angle, and thus give rise to a sharp peak even after integration of $(\partial\sigma/\partial\vartheta)(\vartheta, j')$. For values of $\Delta E/E \simeq 1$, the sharp peak will be broadened but still apparent.

An even more interesting feature is the appearance of two rainbow maxima for systems with additional P_1 or P_4 anisotropy in the interaction potential. For P_1 anisotropy, this is a well-known feature in differential cross sections for collisions involving heteronuclear molecules.[1,8,15] For homonuclear molecules with P_4 anisotropy, this has not yet been identified in experimental cross sections, differential nor integral. In this paper we show that the $Ar(^1S_0) + N_2(C)$ excited-state system is the first likely candidate of this kind, as derived from the bimodal product rotational distribution for the exothermic excitation transfer process $Ar^*(^3P_{0,2}) + N_2(X)$, measured by Nguyen and Sadeghi.[17]

Our discussion is based on classical hard-shell scattering, and will therefore be subject to the usual assumptions and limitations of such a model.[1,9,10,13] In Sec. II, we develop the basic tools required to obtain classical cross sections for rotationally inelastic scattering, with special emphasis on exothermic collisions. In Sec. III we then show that rotational-rainbow maxima are indeed apparent in calculated model cross sections, and discuss their existence in experimental cross sections. In Sec. IV we propose the existence of a double rainbow for homonuclear molecules, an effect caused by potential anisotropy described by a P_4 Legendre polynomial. Section V contains the application of the results of Secs. III and IV to collisions of metastable Ar^* atoms with $N_2(X)$. Finally, in the discussion in Sec. VI, we comment on the qualitative and quantitative value of the model.

II. HARD-SHELL SCATTERING FOR EXOTHERMIC COLLISIONS

The hard-shell scattering model developed by Beck and co-workers[1,9] is a classical approximation to atom-molecule scattering. In this model the following approximations are made. First, obviously any quantal interference is neglected. Second, the treatment of rotational excitation by classical mechanics is valid only in the limit of strong coupling, i.e., when a large number of final rotational states are accessible. This is conveniently expressed by the condition $(E + \Delta E)/B_e \gg 1$, with B_e the rotational constant of the molecule. Third, the molecule is treated as a rigid rotor so any interaction with vibrational states other than the initial state is neglected. Fourth, the full interaction potential is replaced by the equipotential contour for potential energy equal to the collision energy. This last assumption is a high- (radial) velocity approximation, only valid for collisions dominated by short-range repulsion, and with a negligible potential well.

For exothermic collisions, the choice of the equipotential contour is not unambiguous because at least two potential curves are involved, that of the entrance and that of the exit channel. For collisions with a large ratio of exothermicity to collision energy, $\varepsilon = \Delta E/E \gg 1$, the choice can be made by considering that the repulsive action in the exit channel dominates over that in the entrance channel. Therefore, the rotational excitation is mainly due to the final-state interaction, and the hard shell represents an equipotential contour of the repulsive core of the final interaction potential, denoted by $V(\mathbf{R})$.

This equipotential contour can be calculated by inverting the equation

$$V(\mathbf{R}) = E + \Delta E \ , \tag{2}$$

with $\mathbf{R}$ the distance vector from the center of mass of the molecule to the colliding particle. For linear molecules the potential can be expanded in a series of Legendre polynomials P_i according to

$$V(\mathbf{R}) = V_0(R)\left[1 + \sum_{i=1}^{\infty} a_i P_i(\cos\varphi)\right] , \tag{3}$$

with R and φ polar coordinates in the plane through the intramolecular axis and a_i the anisotropy parameters. Here, $V_0(R)$ is the leading term of the repulsive potential. Solving Eq. (2), the equipotential contour is given by

$$R = r_0\left[1 + \sum_{i=1}^{\infty} c_i P_i(\cos\varphi)\right] , \tag{4}$$

with the scaling length r_0 determined by

$$V_0\left[r_0\left[1 + \sum_{i=1}^{\infty} c_i\right]\right] = \frac{E + \Delta E}{1 + \sum_{i=1} a_i} \ . \tag{5}$$

For small anisotropy, $|a_i| \ll 1$, the coefficients c_i are closely related to the anisotropy parameters a_i.

The prescription for calculating a classical cross section is discussed at length by Beck *et al.*[9] In general, the m-fold differential cross section $\Sigma(\boldsymbol{\lambda}_f)$ for excitation of a system described by a set of n initial variables $\boldsymbol{\lambda}_i$ to a state described by a set of m final variables is found by determining all sets of initial variables $\boldsymbol{\lambda}_i$ that lead to the desired $\boldsymbol{\lambda}_f$,

$$\Sigma(\boldsymbol{\lambda}_f) = \int d^n\boldsymbol{\lambda}_i \, \delta(\boldsymbol{\lambda}_f - J(\boldsymbol{\lambda}_i)) \quad (m \le n) \ , \tag{6}$$

where $J(\boldsymbol{\lambda}_i)$ is the excitation function of the system.

In the reduced collision system, we choose as initial variables the momentum $\mathbf{p}$, the impact parameter $\mathbf{b}$, and a unit vector $\mathbf{X}$ describing the orientation of the inter-

molecular axis of the molecule. A body-fixed coordinate system is defined by choosing the z axis along $\mathbf{p}$, and arbitrary x and y axes perpendicular to it. The impact parameter $\mathbf{b}$ is then the xy plane; we denote its angle with the x axis by χ. The direction of $\mathbf{X}$ is defined by polar and azimuthal angles α and γ, respectively:

$$\begin{aligned}\mathbf{p}&=p(0,0,1)\ ,\\ \mathbf{b}&=b(\cos\chi,\ \sin\chi,\ 0)\ ,\\ \mathbf{X}&=(\sin\gamma\cos\alpha,\ \sin\gamma\sin\alpha,\ \cos\gamma)\ .\end{aligned} \tag{7}$$

The coordinate system is shown in Fig. 1. For initially rotating molecules, an initial rotational angular momentum $\mathbf{j}$ exists perpendicular to $\mathbf{X}$; its orientation is described by an angle β with the Z axis of a coordinate system fixed to the rigid shell, with the X axis along $\mathbf{X}$.

As final variables, we are only interested in the length j' of the final rotational angular momentum $\mathbf{j}'$. From Eq. (6) we find that the cross section for rotational excitation of the molecule to all states having rotational angular momentum j' is

$$\sigma(j'\leftarrow j)=\int d\beta\frac{1}{2\pi}\int d(\chi-\alpha)\int b\,db\int\sin\gamma\,d\gamma\,\delta(j'-J(\beta,\chi-\alpha,b,\gamma))\ . \tag{8}$$

Using standard algebra, Eq. (8) can be rewritten in various equivalent ways, always involving the integral of a Jacobian determinant.[9] A useful expression is

$$\sigma(j'\leftarrow j)=\int d\beta\frac{1}{2\pi}\int d(\chi-\alpha)\int\sin\gamma\,d\gamma\times\sum_i\left[\frac{b_i}{|\partial J/\partial b|_{b_i}}\right]\ , \tag{9}$$

where the summation is over all impact parameters b_i that lead to the same final state j' for fixed β, $\chi-\alpha$, and γ. The Jacobian is to be evaluated for fixed β, $\chi-\alpha$, and γ.

All that remains to be defined now is the excitation function J of the hard-shell system. As usual, this is done by evaluating the laws of conservation of angular momentum and total energy at the moment of impact on the shell:

$$\mathbf{j}+\mathbf{r}\times\mathbf{p}=\mathbf{j}'+\mathbf{r}\times\mathbf{p}'\ , \tag{10}$$

$$\frac{j^2}{2I}+\frac{p^2}{2\mu}+\Delta E=\frac{(j')^2}{2I}+\frac{(p')^2}{2\mu}\ . \tag{11}$$

In these equations $\mathbf{p}'$ is the momentum after collision, μ the reduced mass of the system, and I the moment of inertia of the product molecule. The quantity $\mathbf{r}$, the point of impact on the shell, can be evaluated by defining $\mathbf{r}$ to be on the straight-line trajectory $\mathbf{r}=\mathbf{b}+\xi\mathbf{p}$, and choosing ξ such that $\mathbf{r}$ is on the shell. This has to be done numerically, in general.

We note that the essential difference with previous work on the hard-shell model is all contained in the addi-

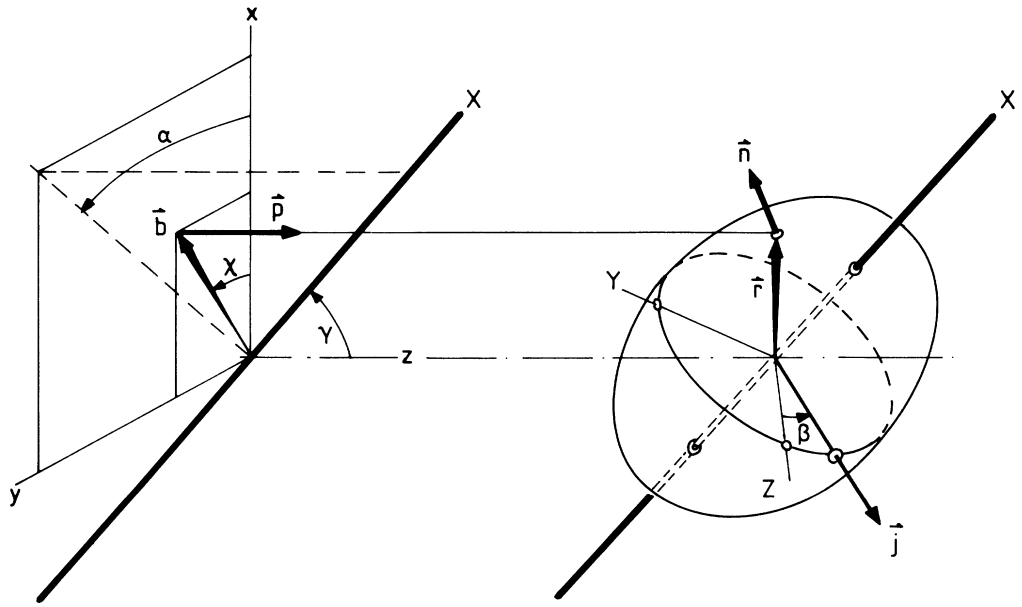

FIG. 1. Visualization of hard-shell scattering. Shown are the figure axis $\mathbf{X}$ of the shell, the initial momentum $\mathbf{p}$, and the impact parameter $\mathbf{b}$, with their directions with respect to the body-fixed coordinate system, xyz. Also shown are the shell-fixed coordinate system XYZ, the point of impact on the shell $\mathbf{r}$, the normal $\mathbf{n}$ on the shell at the point of impact, and the initial rotational angular momentum $\mathbf{j}$.

tion of the energy release ΔE on the left-hand side of Eq. (11). This paper is largely dedicated to the influence of this exothermicity on product rotational distributions. In the following sections, we show that its influence is considerable, eventually leading to the appearance of a classical rotational-rainbow singularity in $\sigma(j' \leftarrow j)$ for large values of the energy release ΔE. This result is very different from integral rotational distributions obtained for collisions without an extra energy release, i.e., with $\Delta E = 0$.

Using $\mathbf{p}' = \mathbf{p} + \Delta p \mathbf{n}$ in Eqs. (10) and (11), with $\mathbf{n}$ the unit vector perpendicular to the shell at the position of impact, we obtain the expression

$$j' = j'_{\max} \left[\frac{\rho r_n}{1+\rho^2 r_n^2} \right] \frac{1}{(1+\varepsilon)^{1/2}} \times \{ p_n + [p_n^2 + \varepsilon(\rho^2 r_n^2 + 1)]^{1/2} \} , \quad (12)$$

with the quantities $j'_{\max}$, ρ, and r_n, and p_n given by

$$j'_{\max} = [2I(E+\Delta E)]^{1/2} ,$$

$$\rho = (\mu/I)^{1/2} r_0 ,$$

$$r_n = \frac{1}{r_0} |\mathbf{r} \times \mathbf{n}| ,$$

$$p_n = (\mathbf{n} \cdot \mathbf{p})/|\mathbf{p}| .$$

We point out that j' depends on initial variables only through p_n, the direction of the impact on the shell, and through r_n, the reduced impact lever. This well-known result[1,9] will prove important in Sec. III, where we investigate the dependence on the exothermicity to collision energy-ratio ε.

III. ROTATIONAL-RAINBOW MAXIMA IN EXOTHERMIC COLLISIONS

Equation (8) is ideally suited for Monte Carlo calculations. The components of $\mathbf{b}$ along the space-fixed x and y axes, the three components of a vector describing the orientation of the rotor-fixed X, Y, and Z axes, and the components of the initial angular momentum $\mathbf{j}$ along the Y and Z axes are all arbitrarily chosen, and the resulting value of j' calculated. The number of shots with a final state j' in the interval $[n\Delta j, (n+1)\Delta j]$ is accumulated in a histogram representing the cross section $\sigma(j')$. Appropriate weights are used to represent, e.g., an initial rotational distribution.

We investigate the influence of the energy release ΔE by calculating integral cross sections for a model system with parameters as in Table I. The initial rotational state is $\mathbf{j} \equiv \mathbf{0}$, and we will denote the resulting cross section by $\sigma(j')$. The important parameter now is the ratio of exothermicity to collision energy,

$$\varepsilon = \frac{\Delta E}{E} = \frac{\Delta E}{p^2/2\mu} . \quad (14)$$

For $\varepsilon = 0$, 2, 10, and infinity, cross sections are shown in Fig. 2. For $\varepsilon = 0$, i.e., no energy release in the second half of the collision, $\sigma(j')$ shows little structure. Already

TABLE I. Model parameters for the hard-shell shape with P_2 anisotropy only (Sec. III).

	P_2 anisotropy
ρ	4
c_2	0.2

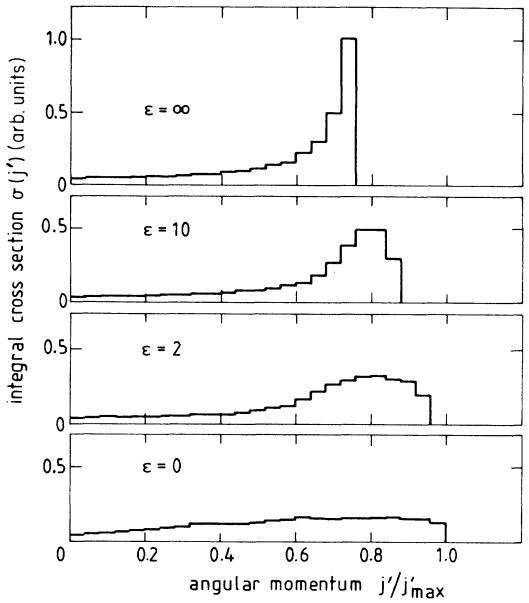

FIG. 2. Integral cross sections for rotational excitation of an initially nonrotating molecule as a function of the scaled final angular momentum j', for various values of the ratio ε of exothermicity to collision energy. They were calculated with the hard-shell scattering model through a Monte Carlo method, and normalized such that the total cross section $\int \sigma(j')dj'$ is the same for each curve. They illustrate that as the exothermicity increases compared to the collision energy, a rotational-rainbow maximum develops at high j', eventually becoming a true, classical singularity for $\varepsilon = \infty$. The parameters of the hard shell are given in Table I.

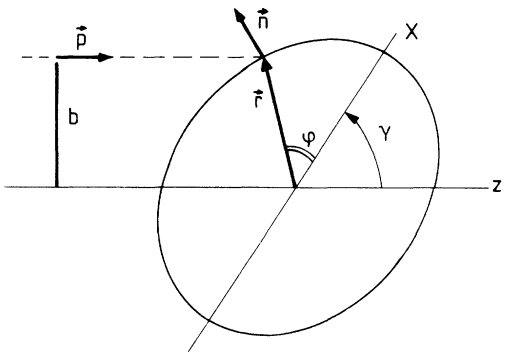

FIG. 3. Visualization of two-dimensional hard-shell scattering for initially nonrotating molecules. The only initial variables are the impact parameter b and the orientation angle γ of the figure axis X of the hard shell with respect to the initial momentum $\mathbf{p}$. Also shown are the point of impact $\mathbf{r}$ and the normal to the shell at the point of impact $\mathbf{n}$. The length of the impact lever r_n, defined in Eq. (13), is determined by the angle ϕ between $\mathbf{r}$ and the figure axis X via the shell shape $R(\phi)$.

for $\varepsilon=2$, however, a maximum develops which grows into a sharp peak at the highest attained state at $\varepsilon=\infty$. This sharp peak resembles the rotational-rainbow singularity encountered in rotationally inelastic cross sections of collisions without energy release at fixed scattering angle.

For very high energy release, i.e., $\varepsilon \gg 1$, we can easily show that the high j' maximum will indeed be a classical rotational-rainbow singularity. Expanding Eq. (12) in ε^{-1} for fixed total energy, i.e., fixed $j'_{\max}$, we find

$$\frac{j'}{j'_{\max}}=\frac{j'_{\infty}}{j'_{\max}}\left[1+\tfrac{1}{2}\varepsilon^{-1}\left[\frac{p_n^2}{1+\rho^2 r_n^2}-1\right]+O(\varepsilon^{-3/2})\right], \tag{15}$$

with the asymptotic value given by

$$\frac{j'_{\infty}}{j'_{\max}}=\left[\frac{\rho^2 r_n^2}{1+\rho^2 r_n^2}\right]^{1/2}. \tag{16}$$

In the limiting case $\varepsilon \gg 1$, the final state j' no longer depends on the direction of impact (p_n), but only on the impact lever r_n. The Jacobian $|\partial j'/\partial b|_{\gamma,\chi-\alpha}$ in Eq. (9) can then be written as

$$\left|\frac{\partial j'}{\partial b}\right|_{\gamma,\chi-\alpha}=\rho^2(1+\rho^2 r_n^2)^{-3/2}\left|\frac{\partial r_n}{\partial b}\right|_{\gamma,\chi-\alpha}, \tag{17}$$

and will have a root at extreme values of the impact lever r_n. These extremal values are, of course, not determined by the initial variables b, $(\chi-\alpha)$, or γ, but only by the shape of the hard shell. The rainbow state j'_R thus does not depend on initial variables. Of course, then the integration of $|\partial j'/\partial b|^{-1}$ over all initial variables to determine the cross section as in Eq. (9) will leave $\sigma(j')$ singular at rainbow states j'_R, corresponding to extreme values of the impact lever r_n.

This is analogous to the rotational-rainbow singularity in differential cross sections for fixed scattering angle and no energy release ($\varepsilon=0$). Beck *et al.*[9] show that both the scattering angle ϑ and the final state j' depend on the initial variables only through the direction of impact p_n and the impact lever r_n. Keeping ϑ fixed, the direction of impact p_n becomes a function of the lever r_n, so the final state j' becomes a function of r_n only. Thus, for fixed scattering angle a rainbow occurs for values of j' corresponding to extreme values of the impact lever r_n. In this case, however, for each ϑ the final state j' is a different function of the lever r_n, so that the rainbow state j'_R depends on the scattering angle.

For moderate energy release, i.e., $\varepsilon \gtrsim 1$, the integral cross section $\sigma(j')$ is no longer singular at the highest attainable state j' because now the rainbow state does depend on the direction of impact p_n. From Eq. (15) it follows, however, that this dependence will still be weak. Therefore, large contributions to $\sigma(j')$ exist for states near the asymptotic rainbow state $j'_{R,\infty}$, where the j'_{∞} distribution has its maximum. Consequently, for $\varepsilon \gtrsim 1$, the cross section has a maximum near the asymptotic rainbow state. This is clearly shown in Fig. 2.

The weak dependence of the rainbow state on initial conditions can easily be demonstrated when we consider the special case of two-dimensional scattering, where the figure axis X is in the plane through **p** and **b**. Now, the only initial variables are the impact parameter b and the orientation of the figure axis with respect to the initial momentum, defined by the orientation angle γ (see Fig. 3). Again, we use the model parameters of Table I.

For $\varepsilon=0$ the final rotational angular momentum j' is plotted as a function of the impact parameter b in Fig. 4(a) for various orientation angles γ. We observe that the rainbow states j'_R, defined by $|\partial j'/\partial b|_{\gamma}=0$, are in the range from zero to the maximum attainable j'. This

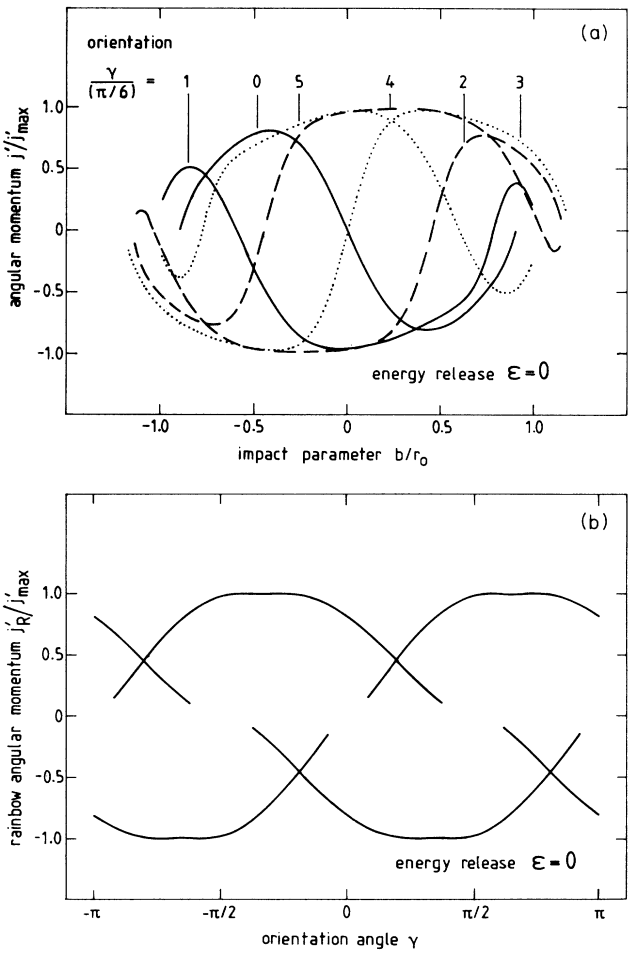

FIG. 4. Dependence of the scaled, final rotational angular momentum j' on the scaled impact parameter b for various orientation angles γ (a) and dependence of the scaled, rainbow-rotational angular momentum j'_R on the orientation angle (b) for two-dimensional scattering with vanishing exothermicity ($\varepsilon=0$). Both figures were calculated with the hard-shell model and the parameters given in Table I. Positive and negative values of j' indicate clockwise and counterclockwise rotation in Fig. 3. Extremal values of j' occur anywhere in the range from zero to the maximum attainable state, depending on the orientation angle γ [Fig. 4(a)], i.e., the rainbow state depends strongly on γ [Fig. 4(b)]. This smears out marked rainbow features, present in the cross sections for fixed orientation angle, when averaging over γ to obtain the integral cross section.

strong dependence of the rainbow state on the orientation angle is more fully shown in Fig. 4(b). Therefore, with no energy release, averaging over all orientation angles smears out the rainbow features present in the cross sections for fixed γ.

For $\varepsilon=10$, however, Fig. 5(a) shows that all orientation angles lead to nearly the same extreme value of j' as a function of the impact parameter b. In Fig. 5(b) where j'_R is plotted as a function of the orientation angle γ, we observe that now the rainbow states are in a narrow range near the asymptotic state $j'_{R,\infty}$. Therefore, for large energy release, the rainbow features in the cross sections for fixed orientation angle shine through in the γ-averaged, integral cross section.

Rotational rainbows in the product rotational distribution of strongly exothermal processes have already been found by Schinke,[14] by Sato *et al.*,[15] and possibly by Cline *et al.*[16] Cline *et al.* did a quantum-mechanical calculation of the vibrational predissociation of $He\cdots Cl_2$ van der Waals molecules to explain the experimental rotational distributions of the product $Cl_2(B)$. Both the calculated and the experimental distributions show a peak near the highest excited j'. Analogous results were obtained for the case of $Ne\cdots Cl_2$.[18] Classical trajectory calculations showed that this peak can be caused by a rotational rainbow, but the rainbow state does not depend as strongly on exothermicity as would be expected.

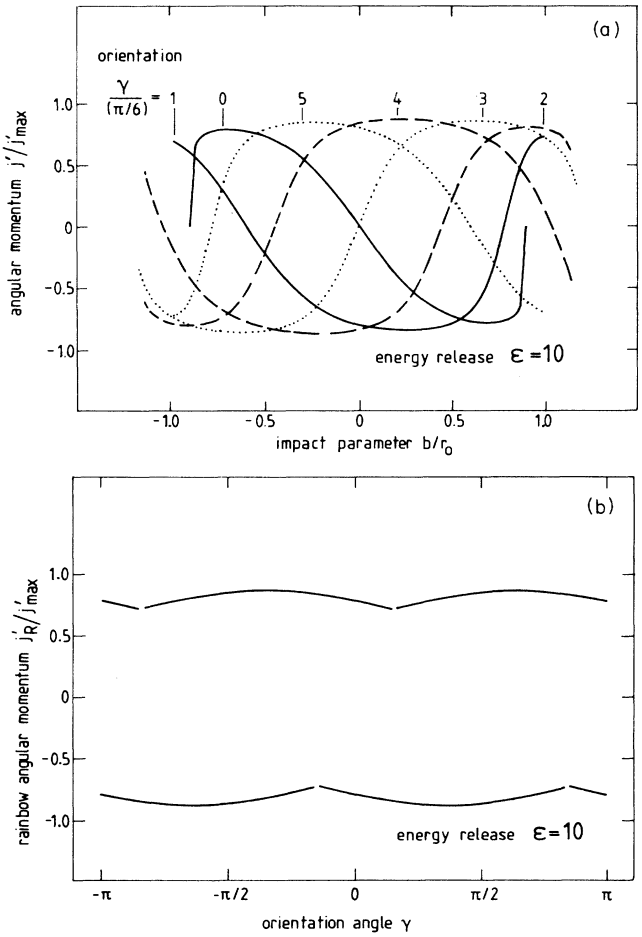

FIG. 5. Same as Fig. 4, but for scattering with large exothermicity compared to collision energy ($\varepsilon=10$). See caption of Fig. 4 for further details. For each orientation angle γ, extremal values of j' occur exclusively in a narrow range around the maximum attainable state [Fig. 5(a)], i.e., the rainbow state depends little on γ [Fig. 5(b)]. This makes marked rainbow features, present in the cross sections for fixed orientation angle, shine through in the γ-averaged, integral cross section.

A clear case is that of the direct photodissociation of H_2CO into H_2+CO, studied by Schinke.[14] With a semiclassical model he calculated the rotational distribution of CO, which showed very good agreement with experimental data of Bamford *et al.*[19] Again, both in the calculated and in the experimental distribution, a maximum at high j' is found. The analysis by Schinke shows that this maximum is definitely caused by a rotational rainbow.

There are also experimental data on rotational distributions of products of exothermic chemical reactions. Billy *et al.*[20] studied the reaction $F+I_2\rightarrow IF+I$ at a collision energy of 110 meV. This is much smaller than the exothermicity of the process, $\Delta E=1.23$ eV. Rotational distributions obtained for various vibrational levels of the product IF all show a maximum at values of j' near the maximum attainable rotational level. Data by Bras *et al.* for the system $Hg+H_2$,[21] and by Breckenridge *et al.* for the system $Mg+H_2$,[22] also show rotational distributions very much resembling those of Fig. 2. Considering the analysis given above, these distributions may well be due to the rotational-rainbow phenomenon, although large allowance has to be made for the specific reaction mechanisms involved.

IV. DOUBLE-RAINBOW DISTRIBUTIONS FOR HETERO- AND HOMONUCLEAR MOLECULES

In Sec. III we showed that rainbow maxima in integral distributions are due to extreme values of the impact lever $r_n=(1/r_0)|\mathbf{r}\times\mathbf{n}|$, just as in the case of rotational distributions of collisions without energy release, measured at fixed scattering angle. Some algebra shows that extreme values of r_n occur when the equation

$$\frac{1}{R}\frac{\partial^2 R}{\partial\varphi^2}+\left[\frac{1}{R}\frac{\partial R}{\partial\varphi}\right]^4=0 \tag{18}$$

is satisfied. For practical purposes, the second term on the left-hand side of this equation can be neglected, because its magnitude is smaller by the third power of the strength of the anisotropy, compared to the first term. Thus, in classical hard-shell scattering, rotational rainbows approximately correspond to a vanishing second derivative $\partial^2R/\partial\varphi^2$, as is exactly true for semiclassical hard-shell scattering.[8]

For an interaction potential with P_0 and P_2 anisotropy, there are two roots $\varphi_1=\pi/4$ and $\varphi_2=3\pi/4$ of this equation for $0\leq\varphi<\pi$. Since

$$P_2(\cos\varphi)=P_2[\cos(\varphi+n\pi/2)] \tag{19}$$

for $\varphi=\pi/4$ and all integer values of n, only one extreme impact lever r_n exists, and thus only one rainbow state.

For heteronuclear molecules, additional P_1 anisotropy may exist. Now, Eq. (18) becomes quadratic in $\cos(\varphi)$ and has two different roots for $0 \leq \varphi < \pi$. Consequently, two different extreme impact levers exist, leading to two rainbow states $j'_{R,1}$ and $j'_{R,2}$. This is a well-known result for collisions with heteronuclear molecules, and was for instance detected by Beck and co-workers[1] in differential energy-loss spectra of K atoms colliding with CO. It has recently been detected by Sato *et al.*[15] in integral distributions of NO atoms following photodissociation of Ar · · · NO and Ne · · · NO van der Waals molecules. These authors find two conspicuous peaks near the maximum rotational state. From the variation of their positions with reduced mass and exothermicity, obtained from experiment as well as quantal calculations, Sato *et al.* conclude that both peaks are due to rotational rainbows. Two peaks might also have been observed in the photodissociation of H_2CO mentioned in Sec. III, but the analysis by Schinke shows that the second maximum is wiped out due to the distribution of bending angles before the dissociation.[14,19]

Although double rainbows are thus a common phenomenon for heteronuclear molecules, they have not been detected for homonuclear molecules. We point out that this is very well possible, however, if higher-order anisotropy of the potential exists. For a homonuclear molecule described by

$$R(\varphi) = r_0[1 + c_2 P_2(\cos\varphi) + c_4 P_4(\cos\varphi)] , \tag{20}$$

the second derivative $\partial^2 R/\partial\varphi^2$ will be quadratic in $\cos^2(\varphi)$. In analogy with the heteronuclear case, now two different values of $\cos^2\varphi$ will make $\partial^2 R/\partial\varphi^2$ singular. Consequently, two extreme impact levers exist, again leading to two rainbow states. The resulting equation is

$$\frac{\partial^2 R}{\partial\varphi^2} = c_2 r_0[70\cos^4\varphi + (6 - \tfrac{135}{2}\delta)\cos^2\varphi + (-3 + \tfrac{15}{2}\delta)] , \tag{21}$$

with $\delta = c_4/c_2$. This equation is singular for two different values of $\cos^2\varphi$ for any value of c_4/c_2.

In Fig. 6 we give the variation of the rainbow states $j'_{R,1}$ and $j'_{R,2}$ as a function of $\delta = c_4/c_2$ for various values of c_2, calculated for a model system with $\alpha = 4$ and large energy release $\varepsilon = 10$. We note that for $\delta \approx 0.3$ the second rainbow state appears at small j', moves toward the main rainbow state for increasing δ, and eventually coincides for $\delta \gg 1$. In the intermediate region, the rainbow states are well separated.

In Fig. 7, we present Monte Carlo calculations of in-

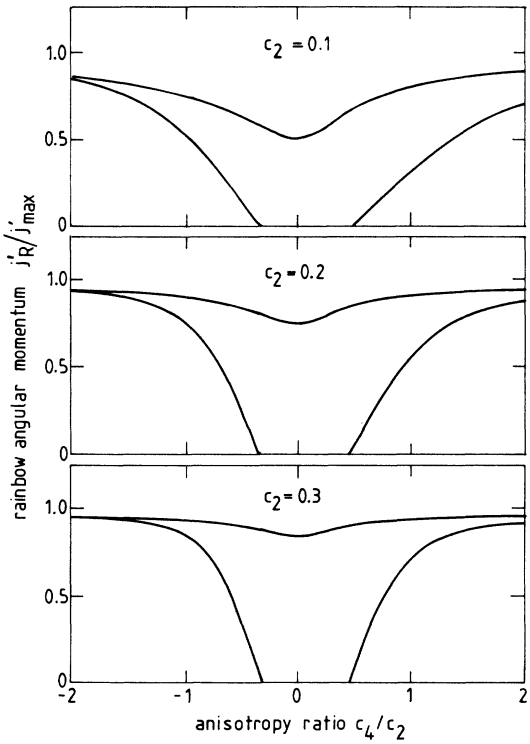

FIG. 6. Dependence of the two scaled rainbow angular-momentum states, $j'_{R,1}$ and $j'_{R,2}$ for a two-dimensional system with P_2, P_4 anisotropy, on the ratio of anisotropies c_4/c_2, for various values of c_2. The ratio of exothermicity to collision energy is $\varepsilon \gg 1$, and the hard-shell parameter $\rho = 4$. In the range $0.3 < c_4/c_2 < 1$, the two rainbows states are well separated.

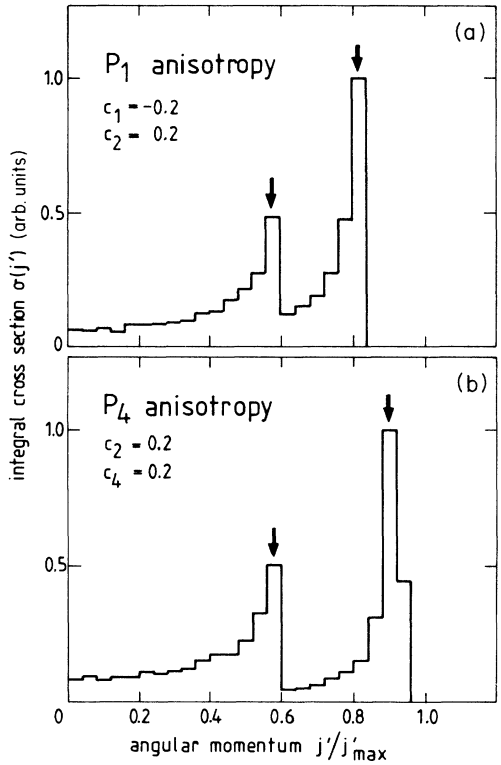

FIG. 7. Integral cross sections for rotational excitation showing two rotational rainbows (indicated by the arrows), for a heteronuclear molecule with P_1, P_2 anisotropy (upper figure), and for a homonuclear molecule with P_2, P_4 anisotropy (lower figure). Both were calculated for a very large ratio of exothermicity to collision energy ($\varepsilon \gg 1$). The anisotropy parameters are indicated in the figure; all hard-shell parameters are listed in Table II. In both cases, the two rainbows are well separated and of comparable intensity.

TABLE II. Model parameters for the hard-shell shapes with P_1,P_2 anisotropy, representing a heteronuclear molecule, and with P_2,P_4 anisotropy, representing a homonuclear molecule. These shapes were used to calculate the double-rainbow cross sections shown in Fig. 7.

	P_1,P_2 anisotropy	P_2,P_4 anisotropy
ρ	4	4
c_1	−0.2	0
c_2	0.2	0.2
c_4	0	0.2

tegral cross sections for the model system under investigation, for both (P_1,P_2) and (P_2,P_4) anisotropy. The parameters are given in Table II. We note that in the heteronuclear as well as in the homonuclear case, the two rainbows are well separated and of comparable intensity.

Of course, adding even higher-anisotropy terms such as P_3 and P_8 we can create any number of classical rotational rainbows for suitable choices of the parameters. However, quantum mechanically, rotational-rainbow maxima are much broader than the sharp, classical singularities. Therefore only a limited number of rainbows can be seen, even if interference between the various rainbow states is neglected. Systems with many rainbows may be classically feasible, but these rainbows are probably not real.

To our knowledge, a double-rainbow maximum in the rotational distribution of a homonuclear molecule has not yet been identified, neither in a differential nor in an integral distribution. For ground-state molecules, probably P_2 anisotropy is always dominant, but for excited molecules this is not *a priori* true. In Sec. V we investigate the possibility that the excited system $\mathrm{Ar}(^1S_0)+\mathrm{N}_2(C)$ shows the double-rainbow feature just established.

V. HIGHER-ORDER ANISOTROPY FOR THE EXCITED SYSTEM $\mathrm{Ar}(^1S_0)+\mathrm{N}_2(C)$

We now turn to the process

$$\mathrm{Ar}^*(^3P_{0,2})+\mathrm{N}_2(X)\rightarrow\mathrm{Ar}(^1S_0)+\mathrm{N}_2(C,v')+\Delta E\ , \qquad (22)$$

which has become a prototype of exothermal excitation transfer collisions. The exothermicity is $\Delta E=701$ meV for $\mathrm{Ar}^*(^3P_0)$ and final vibrational state $v'=0$, and $\Delta E=526$ meV for $\mathrm{Ar}^*(^3P_2)$. Various aspects of this process received extensive attention, both experimentally and theoretically.[17,23–27] In this paper we focus on the rotational distribution of the product molecule $\mathrm{N}_2(C)$ and investigate the possibility that it shows the double-rainbow effect pointed out in Sec. IV.

There are two recent sources of information about this distribution. The first is a bulk experiment performed by Nguyen and Sadeghi[17] at temperatures of 90 and 300 K (collision energy $E=11$ and 39 meV, respectively). For the vibrational state $v'=0$, they resolved the rotational structure in the spectrum of the decay $\mathrm{N}_2(C)\rightarrow\mathrm{N}_2(B)$ as well as state-selected the $\mathrm{Ar}^*(^3P_{0,2})$ metastable atoms. For initial state $\mathrm{Ar}^*(^3P_2)$ and a temperature of 90 K, the cross section calculated from the experimental spectrum extends to rotational level $j'=48$, the highest rotational level that can be reached on the grounds of energy conservation. Surprisingly, the cross section has maxima at two different values of the final rotational angular momentum, denoted as $j'_1=22$ and $j'_2=37$. For $\mathrm{Ar}^*(^3P_0)$, the rotational distribution is similar but shifted to higher values of j' by an amount $\Delta j'\simeq 6$. For both states the maximum at high j' is less clear at 300 than at 90 K. In their paper, Nguyen and Sadeghi show that these "bimodal" rotational distributions cannot be explained by common, statistical models of rotational excitation.[17]

The second and more qualitative source of information is the rotationally unresolved spectrum of the decay $\mathrm{N}_2(C)\rightarrow\mathrm{N}_2(B)$ reported by van Vliembergen *et al.*[23] Their experimental spectrum can be reasonably simulated by assuming Boltzmann distributions for the rotational populations of the vibrational levels $v'=0$–3, with effective "temperatures" up to as high as 2000 K for $v'=0$. However, deviations from these distributions, denoted "humps" by van Vliembergen *et al.*, are apparent in the spectrum. These "humps" represent high rotational levels more populated than follows from the calculated Boltzmann distribution, and their presence confirms the observation of two maxima in the rotational distributions mentioned above. Furthermore, the position $j'=37$ of the "hump" in the spectrum originating from the $v'=0$ level agrees with the position of the maximum of the high-j' component in the rotational distribution obtained by Nguyen and Sadeghi.[17]

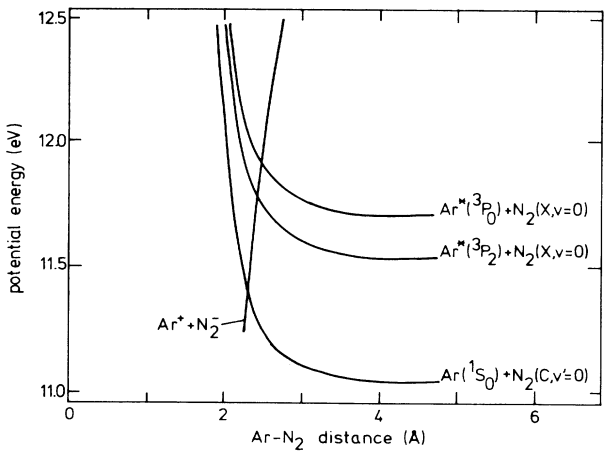

FIG. 8. Semi-empirical potential curves for the exothermic excitation transfer process $\mathrm{Ar}^*(^3P_{0,2})+\mathrm{N}_2(X)\rightarrow\mathrm{Ar}(^1S_0)+\mathrm{N}_2(C,v'=0)$, proposed by van Vliembergen *et al.* (Ref. 23). The initial and final states are connected via two curve crossings with the ionic intermediate potential of the system $\mathrm{Ar}^+(^2P)+\mathrm{N}_2^-(X)$. Of this potential, only the Coulomb part is shown. The curve crossing of the initial state $\mathrm{Ar}^*(^3P_2)+\mathrm{N}_2(X)$ with the intermediate potential occurs at an unrealistically high energy (see text), indicating a much flatter entrance potential than shown in the figure.

The interaction potentials for the system are not well known. However, realistic semiempirical potential curves were proposed by van Vliembergen *et al.*[23] and are reproduced in Fig. 8. They show initial and final states connected through two curve crossings with the ionic $Ar^+ + N_2^-$ potential as an intermediate. Of the ionic potential, only the Coulomb part is shown. Because of short-range repulsion, this curve must bend upward toward smaller internuclear distance, which will make the curve crossing with the final state occur on the repulsive part of the final-state potential. For the potentials shown, the curve crossing with the initial state occurs at an energy $E = 225$ meV with respect to the initial asymptote. This value is unrealistic. Recent measurements from our own laboratory[28] point towards a threshold of 65 meV. Measurements of Parr and Martin[26] lead to an even lower value of 8 meV, while Sanders *et al.*[27] find a threshold of about 50 meV. These differences may be due to different $Ar(^3P_0)$:$Ar(^3P_2)$ beam compositions, which were unknown for all experiments. All data sets do point to a substantially lower threshold, however, than given by the potential curves of van Vliembergen *et al.* This indicates a much flatter entrance potential than shown in Fig. 8. Our measurements are further consistent with a second curve crossing located on the repulsive branch of the final-state potential, such that at least 60% of the exothermic energy is released after the second curve crossing is reached.[28]

These two facts, a low threshold and a large repulsive-energy release, indicate that the system $Ar^* + N_2$ behaves as the half-collisions analyzed in Sec. III. We therefore expect at least one rainbow maximum in the rotational distribution of the product $N_2(C)$. In view of the result of Sec. IV, the bimodal distribution measured by Nguyen and Sadeghi can be explained as a double-rainbow distribution caused by a substantial P_4 anisotropy.

In Fig. 9 we compare the experimental cross section obtained by Nguyen and Sadeghi[17] for the initial state $Ar^*(^3P_2)$ and a temperature of 90 K with a "best fit" of a model cross section including P_4 anisotropy. The parameters are given in Table III. The positions of the rainbow peaks can easily be made to coincide with the experimental data. Also shown is a cross section obtained with the same model, but extended to include a 90-K initial rotational distribution. The latter cross section was obtained from that for zero initial rotation using the factorization formula of Parker and Pack,[8,30]

$$\sigma(j' \leftarrow j) = \sum_{\Delta j} (j0\,\Delta j0 | j'0)^2 \sigma(\Delta j' \leftarrow 0) , \tag{23}$$

with $(j0\Delta j0|j'0)$ a Clebsch-Gordan coefficient. Summing over all initial rotational states we get

$$\sigma(j') = \sum_j \sum_{\Delta j} g(j)(j0\,\Delta j0 | j'0)^2 \sigma(j' \leftarrow 0) , \tag{24}$$

with

$$g(j) = (2j/\hbar + 1) e^{-j^2/(2IkT)} \tag{25}$$

a Boltzmann distribution for a temperature $T = 90$ K. We could equally well include the initial Boltzmann distribution in the Monte Carlo calculation, as indicated in Sec. II. We find, however, that the result is close to that obtained with Eq. (24).

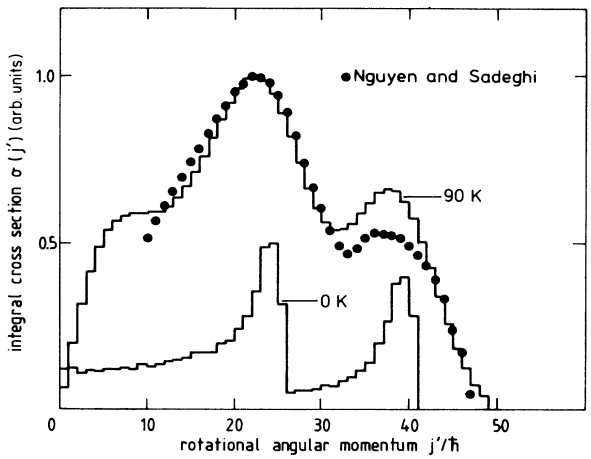

FIG. 9. Comparison of experimental and calculated integral cross sections for rotational excitation of N_2 in the excitation transfer process $Ar^*(^3P_2) + N_2(X) \rightarrow Ar(^1S_0) + N_2(C, v' = 0)$, vs final rotational angular momentum. The points indicate experimental data taken from the rotational distribution given by Nguyen and Sadeghi (Ref. 17), identifying the rotational quantum number with $j'/\hbar$. The solid curves show cross sections calculated with the hard-shell model and the parameters in Table III. The lower curve corresponds to initially nonrotating molecules, while the upper curve incorporates initial rotation given by a 90-K Boltzmann distribution. Given the simplicity of the model, the degree of agreement with the experimental data points is somewhat fortuitous.

With the inclusion of an initial rotational distribution, we find that the rainbow peaks are broadened in such a way that now the calculated cross section gives a fair overall representation of the experimental data. Considering the simplicity of the model, the degree of agreement is somewhat fortuitous. With an initial rotational tem-

TABLE III. Constants and model parameters for the process $Ar^*(^3P_2) + N_2(X) \rightarrow Ar(^1S_0) + N_2(C, v' = 0)$. The hard-shell parameters were used to calculate the double-rainbow cross section shown in Fig. 9.

Constants	
E (meV)	11[a]
ΔE (meV)	521
$(\mu/I)^{1/2}$ (Å^{-1})	1.33[b]
Hard-shell parameters	
j_0' ($\hbar$)	48
ε	51
r_0 (Å)	3.0
ρ	4.0
c_2	0.06
c_4	0.11

[a]Corresponding to a bulk temperature of 90 K.
[b]Calculated using the rotational constant given by Herzberg (Ref. 29).

TABLE IV. Experimental and calculated positions j'_1 and j'_2 (in units of $\hbar$) of the two rainbow maxima in the integral cross section for rotational excitation of $N_2(C)$ following the excitation process $Ar^*(^3P_{0,2})+N_2(X)$, for both metastable states $Ar^*(^3P_0)$ and $Ar^*(^3P_2)$ and for the temperature of 90 K. The parameters of the hard-shell model are given in Table III. The experimental positions were taken from the rotational distribution shown by Nguyen and Sadeghi (Ref. 17), identifying the rotational quantum number by $j'/\hbar$.

			Experimental		Hard-shell model	
	E (meV)	ΔE (meV)	j'_1	j'_2	j'_1	j'_2
$Ar^*(^3P_2)+N_2(X)$	11	521	22	37	22	37
$Ar^*(^3P_0)+N_2(X)$	11	701	26	45	25	43

perature of 300 K, the model cross section becomes broadened too much to describe the data of Nguyen and Sadeghi for this temperature. In Table IV we compare the positions of the rainbow maxima calculated with the model parameters of Table III for both initial states $Ar^*(^3P_0)$ and $Ar^*(^3P_2)$, with the experimental positions. We find that the shift $\Delta j' \approx 6$, in going from $Ar^*(^3P_2)$ to $Ar^*(^3P_0)$, is adequately described by the model.

VI. DISCUSSION AND CONCLUSIONS

In this paper we showed that for exothermic collisions rotational-rainbow maxima should be a common feature in product rotational distributions. Our discussion is based on the classical rigid-shell scattering model developed by Beck and co-workers,[1,9] adapted to the situation. We expect our conclusions to have definite qualitative value, because the hard-shell model has been proven to be qualitatively correct for product rotational distributions of collisions without energy release, obtained at fixed scattering angle: rotational rainbows have been detected for a number of such processes.[8] The quantitative value of this model depends on the quantity studied, however. Anisotropy parameters, determined from experimental rainbow positions with the classical rainbow curve $j'_R(\vartheta)$, given by Bosanac[31] and Bosanac and Buck[32] for ellipsoidal and off-center ellipsoidal potential shells, respectively, show fair agreement with the anisotropy of the full potentials.[33] Also, the dependence of the rainbow position on the scattering angle, reduced mass, and collision energy are adequately predicted by the model.[8]

On the other hand, Korsch and Schinke demonstrated that the model greatly underestimates the cross section for transitions with a small value of $j'-j$ and for small-angle scattering.[10] For integral cross sections, Alexander and Dagdigian[13] as well as Korsch and Schinke[10] find that the model utterly fails when compared to quantal and semiclassical calculations. Korsch and Schinke argue that both these failures are due to the approximation of a hard shell. Because of the unrealistic radial dependence of the "potential," the contributions of large impact parameters, which are responsible for most of the low $j' \leftarrow j$ transitions and lead to small scattering angles, are not included.

This probably does not invalidate rotational populations calculated with the model for exothermic collisions, however. First, the large energy release, in comparison to the collision energy, ensures that exothermic collisions are always strongly repulsive in nature. Therefore, small $j' \leftarrow j$ transitions are not likely, and the scattering is mostly backward. Second, large impact parameters do not contribute strongly to exothermic collisions because, for nonadiabatic collisions, a curve crossing must be reached, and for reactive collisions, a transition state must be reached. Both will be located at smaller internuclear distances, because an amount of energy must be released through repulsive interaction.

In Sec. II we limited ourselves to collisions with little repulsive or attractive action in the entrance channel. We now point out that this restriction can be somewhat released. Non-negligible interaction in the entrance channel causes deviations of the straight line trajectories inherent in the hard-shell model. This changes the point of impact on the shell and has to be taken into account on the right-hand side of Eq. (10) from which j' is calculated. However, this does not change the left-hand sides of Eqs. (10) and (11) because these represent the total angular momentum and the total energy at the start of the collision. Therefore, the dependence of the final rotational angular momentum on the initial variables may change, in turn changing the rotational distribution but

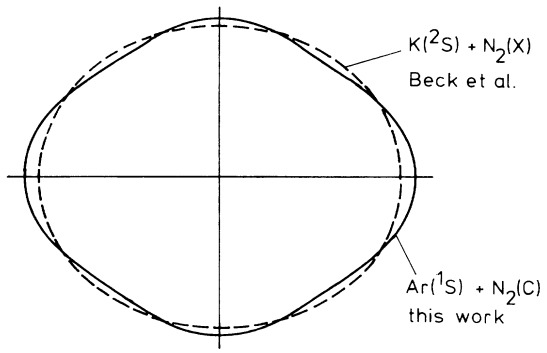

FIG. 10. Angular dependence $R(\phi)/r_0$ of hard-shell shapes. The dashed curve indicates the shape used by Beck *et al.* (Ref. 9) to explain experimental data on rotational excitation of $N_2(X)$ by collisions with ground-state $K(^2P)$ atoms. The solid curve represents the P_2, P_4 anisotropic shape used in this work to explain the rotational distribution of the product $N_2(C)$ of the excitation transfer process $Ar^*(^3P_{0,2})+N_2(X)$, measured by Nguyen and Sadeghi (Ref. 17). The bulge of the latter shape, located perpendicular to the figure axis, may indicate a shift of the electron density to the plane perpendicular to the N-N axis, caused by the promotion of an $N_2(2\sigma_u)$ electron to a $2\pi_g$ orbital.

not changing the position of the rainbow state, since this only depends on the shape of the shell, the total angular momentum, and the total energy. Thus, strong contributions to the rotational distribution will still exist for values of j' close to the rainbow state j'_R. Unless the initial-state interaction completely changes the trajectories in such a way that the rainbow rotational transition can never be excited, at least a small peak will be visible in the product rotational distribution.

In our application of the double-rainbow model to the rotational distribution of $N_2(C)$ obtained by Nguyen and Sadeghi[17] for the excitation transfer process $Ar^*(^3P_{0,2})+N_2(X)$ fair agreement is obtained between experimental and calculated results for a temperature of 90 K. For 300 K, the calculated distribution is broader than the experimental. The value of the parameters in the model cannot be readily assessed, however. A comparison with the parameters of Beck *et al.*[9] for the system $K+N_2$, $r_0=2.5$ Å, and $c_2=0.078$ only shows that our values are not unreasonable. For the strength of the P_4 term, there is no material to compare with. It is not unlikely that a contribution of such a potential term exists for the excited molecule $N_2(C)$. The excitation of $N_2(X)$ to $N_2(C)$ during the collision of Eq. (22) requires an antibonding $N_2(2\sigma_u)$ orbital to be promoted to a $N_2(2\pi_g)$ orbital; this can be described as a two-step process.[24] The result is that the charge density of the antibonding orbital is shifted to the plane perpendicular to the N-N axis of $N_2(C)$. Such a shift of the electron density is partly described by the addition of a P_4 anisotropy. In Fig. 10 we show the equipotential contour described by the model parameters. We note that the P_4 term has caused a bulge in the direction perpendicular to the N-N axis, which can be interpreted as a shift of the electron density to this plane.

More experimental data are needed to irrefutably assign the bimodal distribution of $N_2(C,v'=0)$ to the double-rainbow effect. For instance, the dependence of the rotational distribution on collision energy and on exothermicity, i.e., final vibrational level v', can be measured. Also, it would be interesting to investigate the effect of P_4 anisotropy through more quantitative calculations. For complicated systems such as Ar^*+N_2, probably only classical trajectory calculations are feasible. The work by Schinke on the "rotational reflection principle"[34] shows that these can have quantitative value, however. Such work could also explain exactly why no double rainbow is encountered in the differential cross sections for the scattering of He by Na_2, calculated by Schinke,[11(b)] though the expansion of the interaction potential in Legendre polynomials shows a strong contribution of P_4 anisotropy at small intermolecular distances. Most likely, this is due to the simultaneous rise of even higher-order anisotropic terms, accompanying the rise of the P_4 term. This will lead to very different equipotential contours than the (P_2,P_4) shape we used for the system $Ar(^1S_0)+N_2(C)$.

*Present address: Océ Nederland B.V., P.O. Box 101, 5900 MA Venlo, The Netherlands.

[1]W. Schepper, U. Ross, and D. Beck, Z. Phys. A **290**, 131 (1979); D. Beck, U. Ross, and W. Schepper, Phys. Rev. A **19**, 2173 (1979).

[2]K. Bergmann, U. Hefter, and J. Witt, J. Chem. Phys. **72**, 4777 (1980); E. Gottwald, A. Mattheus, and K. Bergmann, *ibid.* **86**, 2680 (1987).

[3]E. Gottwald, K. Bergmann, and R. Schinke, J. Chem. Phys. **86**, 2685 (1987).

[4]G. Ziegler, M. Rädle, O. Pütz, K. Jung, H. Ehrhardt, and K. Bergmann, Phys. Rev. Lett. **58**, 2642 (1987).

[5]For a review of ion-molecule scattering, see M. Faubel and J. P. Toennies, Adv. At. Mol. Phys. **13**, 229 (1977).

[6]For a review of atom-molecule scattering, see H. G. Loesch, Adv. Chem. Phys. **42**, 421 (1980).

[7]J. Andres, U. Buck, H. Meyer, and J. M. Launay, J. Chem. Phys. **76**, 1417 (1982); R. Schinke, H. Meyer, U. Buck, and G. H. F. Diercksen, *ibid.* **80**, 5518 (1984).

[8]For a review of rotational-rainbow scattering, see R. Schinke and J. M. Bowman, in *Molecular Collision Dynamics*, edited by J. M. Bowman (Springer, Berlin, 1983).

[9]D. Beck, U. Ross, and W. Schepper, Z. Phys. A **293**, 107 (1979); **299**, 97 (1979).

[10]H. J. Korsch and R. Schinke, J. Chem. Phys. **75**, 3850 (1981).

[11](a) H. J. Korsch and R. Schinke, J. Chem. Phys. **73**, 1222 (1980); (b) R. Schinke, W. Müller, W. Meyer, and P. McGuire, *ibid.* **74**, 3916 (1981); (c) H. J. Korsch and D. Poppe, Chem. Phys. **69**, 99 (1982).

[12]R. Schinke, J. Chem. Phys. **72**, 1120 (1980).

[13]M. H. Alexander and P. J. Dagdigian, J. Chem. Phys. **73**, 1233 (1980).

[14]R. Schinke, Chem. Phys. Lett. **120**, 129 (1985).

[15]K. Sato, Y. Achiba, H. Nakamura, and K. Kimura, J. Chem. Phys. **85**, 1418 (1986).

[16]J. I. Cline, B. P. Reid, D. W. Evard, N. Savikumar, N. Halberstadt, and K. C. Janda, J. Chem. Phys. **89**, 3535 (1988).

[17]T. D. Nguyen and N. Sadeghi, Chem. Phys. **79**, 41 (1983).

[18]J. I. Cline, N. Sivakumar, D. W. Evard, and K. C. Janda, J. Chem. Phys. **86**, 1636 (1987); N. Halberstadt, J. A. Beswick, and K. C. Janda, *ibid.* **87**, 3966 (1987).

[19]D. J. Bamford, S. V. Filseth, M. F. Foltz, J. W. Hepburn, and C. B. Moore, J. Chem. Phys. **82**, 3032 (1985).

[20]N. Billy, B. Girard, G. Gouedard, and J. Vigue, J. Chem. Phys. **88**, 2342 (1988).

[21]N. Bras, J. Butaux, J. C. Jeannet, and D. Perrin, J. Chem. Phys. **85**, 280 (1986).

[22]W. H. Breckenridge and H. Umemoto, J. Chem. Phys. **80**, 4168 (1984); W. H. Breckenridge and J.-H. Wang, Chem. Phys. Lett. **137**, 195 (1987).

[23]E. J. W. van Vliembergen, E. J. D. Vredenbregt, G. H. Kaashoek, J. P. M. J. Jaspar, M. M. M. van Lanen, M. F. M. Janssens, M. J. Verheijen, and H. C. W. Beijerinck, Chem. Phys. **114**, 117 (1987).

[24]G. W. Tyndall, M. S. de Vries, C. L. Cobb, and R. M. Martin, J. Chem. Phys. **87**, 5830 (1987).

[25]An extensive list of references is given in Ref. 24.
[26]T. P. Parr and R. M. Martin, J. Chem. Phys. **69**, 1613 (1978).
[27]R. A. Sanders, A. N. Schweid, M. Weiss, and E. E. Muschlitz, Jr., J. Chem. Phys. **65**, 2700 (1976).
[28]W. Boom, EUT Internal Report No. VDF/NO 88-16, Eindhoven (1988) (in Dutch).
[29]G. H. Herzberg, *Molecular Spectra and Molecular Structure* (Van Nostrand/Reinhold, New York, 1950), Vol. I.
[30]G. A. Parker and R. T. Pack, J. Chem. Phys. **68**, 1585 (1978).
[31]S. Bosanac, Phys. Rev. A **22**, 2617 (1980).
[32]S. Bosanac and U. Buck, Chem. Phys. Lett. **81**, 315 (1981).
[33]U. Buck, Comments At. Mol. Phys. **17**, 143 (1986).
[34]R. Schinke, J. Chem. Phys. **85**, 5049 (1986).